An analytical study of tribological parameters between piston ring and cylinder liner in internal combustion engines

Article *in* Proceedings of the Institution of Mechanical Engineers Part K Journal of Multi-body Dynamics · October 2015

DOI: 10.1177/1464419315605922

CITATIONS
45

READS
20,853

4 authors, including:

Mohamed Kamal Ahmed Ali
Minia University
76 PUBLICATIONS **2,770** CITATIONS

SEE PROFILE

Richard Fiifi Turkson
Ho Technical University
21 PUBLICATIONS **859** CITATIONS

SEE PROFILE

Original Article

Institution of MECHANICAL ENGINEERS
Journal of MULTI-BODY DYNAMICS

Proc IMechE Part K:
J Multi-body Dynamics
0(0) 1–21

DOI: 10.1177/1464419315605922
pik.sagepub.com
SAGE

An analytical study of tribological parameters between piston ring and cylinder liner in internal combustion engines

Mohamed Kamal Ahmed Ali[1,2], Hou Xianjun[1], Richard Fiifi Turkson[1,3] and Muhammad Ezzat[4]

Abstract

This paper presents a model to study the effect of piston ring dynamics on basic tribological parameters that affect the performance of internal combustion engines by using dynamics analysis software (AVL Excite Designer). The paramount tribological parameters include friction force, frictional power losses, and oil film thickness of piston ring assembly. The piston and rings assembly is one of the highest mechanically loaded components in engines. Relevant literature reports that the piston ring assembly accounts for 40% to 50% of the frictional losses, making it imperative for the piston ring dynamics to be understood thoroughly. This analytical study of the piston ring dynamics describes the significant correlation between the tribological parameters of piston and rings assembly and the performance of engines. The model was able to predict the effects of engine speed and oil viscosity on asperity and hydrodynamic friction forces, power losses, oil film thickness and lube oil consumption. This model of mixed film lubrication of piston rings is based on the hydrodynamic action described by Reynolds equation and dry contact action as described by the Greenwood–Tripp rough surface asperity contact model. The results in the current analysis demonstrated that engine speed and oil viscosity had a remarkable effect on oil film thickness and hydrodynamic friction between the rings and cylinder liner. Hence, the mixed lubrication model, which unifies the lubricant flow under different ring–liner gaps, is needed via the balance between the hydrodynamic and boundary lubrication modes to obtain minimum friction between rings and liner and to ultimately help in improving the performance of engines.

Keywords

Internal combustion engines, piston ring dynamics, boundary lubrication friction, hydrodynamic friction, lube oil consumption

Date received: 14 June 2015; accepted: 18 August 2015

Introduction

The tribological behavior of piston and rings assembly has long been recognized as an important influence on the performance of internal combustion engines in terms of fuel consumption, power loss, oil consumption, harmful exhaust emissions and blow-by.[1] Different friction mechanism scenarios may occur due to the sliding action between the piston ring and the cylinder liner during one working cycle of the engine, mainly because of the variations in speed, load, and counter surface effects.[2] Figure 1 shows a distribution of the total engine mechanical friction losses for a diesel engine. It was observed that the largest part of friction losses in the engine was at the piston and ring assembly.[3] Frictional power losses for the Mercedes Benz engine were distributed as follows: piston ring assembly 40%, bearings 35%, and valve train 25%. These results were for an SAE 30 mono-grade and an engine speed of 2500 r/min during a medium engine load.[4] The total friction between piston rings and cylinder liner can be addressed as hydrodynamic friction because of lubricant shearing and boundary film

[1]Hubei Key Laboratory of Advanced Technology for Automotive Components, Wuhan University of Technology, Wuhan, China
[2]Automotive and Tractors Engineering Department, Faculty of Engineering, Minia University, Egypt
[3]Mechanical Engineering Department, Ho Polytechnic, Ghana
[4]Institute of Technology, University of Ontario, Ontario, Canada

Corresponding author:
Mohamed Kamal Ahmed Ali, Hubei Key Laboratory of Advanced Technology for Automotive Components, Wuhan University of Technology, Wuhan 430070, China.
Email: Eng.m.kamal@mu.edu.eg

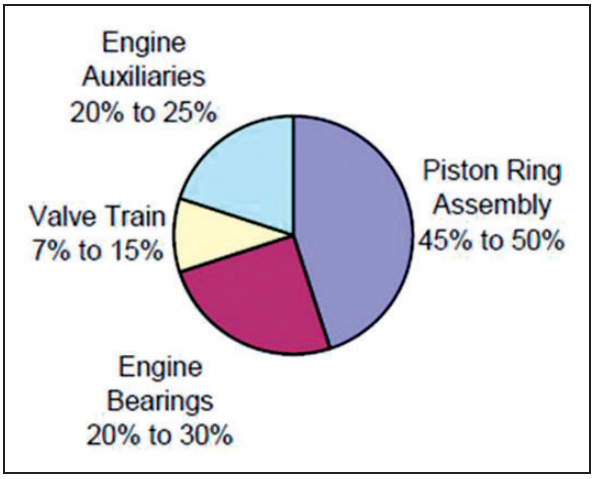

Figure 1. Distribution of the total mechanical losses of a diesel engine as given by Comfort.[3]

friction at asperity contact locations.[5] The negative aspects of the friction force variation with the crank angle would be due to the change of piston speed direction through the reciprocating motion.[6] Experiments conducted by Takiguchi et al.[7] with two-ring and three-ring pistons indicated that the number of rings influenced the frictional behavior. However, the piston friction force can be reduced regardless of the number of piston rings, by reducing the total tension of piston rings, but the lowered tension of oil ring results directly in the increase of lubrication oil consumption. With increasing engine speed the excitement frequency changes, as well as the exciting force. This is because the friction forces strongly depend on the engine speed. With rising engine speed the shear stress also increases and with it, the friction force.[8]

The high temperature and low viscosity of lubrication oil at the end of compression stroke and the beginning of the expansion stroke at the top dead center (TDC) result in the most severe lubrication conditions that occur, especially for the top ring.[9] In boundary lubrication, the depressions acts as a storage for supplying lubricant inside the contact during sliding, whereas the depressions in the full oil film increase the hydrodynamic effect of the lubricant.[10] Loading variation sometimes has a negative influence on frictional power. An example of this is the top ring surface frictional power being increased with increasing load. Furthermore, the loading variation does not affect the frictional power at other rings due to the low gas pressure on the backside of the rings, which is mainly because of the sealing capability of the first compression ring.[11] Xu et al.[12] compared different diesel fuels and examined their effect on the tribological properties of a piston and ring assembly. Results from the study indicated that the piston and ring assembly lubricated with bio-oil had a lower friction coefficient due to the adsorption of polar groups of carboxylic acids and alcohols on the rubbing surface, but had a higher wear mass and greater surface roughness than the piston and ring assembly lubricated with diesel oil. Peak values of friction coefficient at TDC and bottom dead center (BDC) locations were in the range of 0.10 to 0.15 and mid-stroke values ranging from 0.05 to 0.10. The values depend on the surface quality, actual lubricant and surface material.[13] A piston ring may experience boundary, mixed, and full fluid film lubrication in one single stroke.[14] Douglas et al.[15] studied the tribological behavior of piston ring assembly in diesel engines using an acoustic emission (AE) sensor to discuss the possible AE source mechanisms, such as lubricant flow, asperity contact and measure the oil film between piston rings and cylinder liner. The experimental results showed that an increase in oil film thickness with increasing piston speeds. Friction coefficient, frictional force, and wear reduced with the use of the bio-lubricant compared with the other lubricants. The reduction was because of the presence of oxygenated moieties and the double bonds in biodiesel led to an additional improvement in the overall lubricity of biodiesel contaminated lubrication oil.[16] Boundary, mixed, and hydrodynamic lubrication regimes can occur at different points in the stroke. Mixed and boundary lubrication regimes show the highest friction and occur near TDC and BDC.[17]

The friction coefficient is dependent upon the value of the oil film thickness between the piston rings and cylinder liner, cylinder pressure, speed, oil effective viscosity, and ring–liner temperature. The increase in the gas pressure on the piston ring and the decrease of the oil viscosity causes a decrease in the oil film thickness between ring and liner.[18] Takata and Rosalind Rosalind Kazuko[19] studied the effect of lubricant viscosity influence throughout the engine cycle, the study specified the mid-stroke region as the main impact (compared to the end-strokes) on frictional power losses, and a reduction in ring-pack FMEP about 7% could be achieved if oil viscosity is reduced. Moreover, slow of piston speeds cause asperity contact to be high at the end strokes (TDC and BDC), resulting in high wear rates at TDC and BDC. The friction mean effective pressure (FMEP) is not much affected by these asperity contacts because they occur close to TDC where piston velocity is low.[20] The oil film thickness calculations and measurements by Richardson and Borman reveal that the theoretical value of the oil film thickness at the beginning of the downward stroke did not match the actual measurements since the measured showed higher values compared with the theoretical ones. This difference in values was attributed to the additional oil transported from the piston skirt and piston slap-motion, which prevents the oil ring from following the cylinder liner.[21,22] Reducing the ring tangential tension increases the oil film thickness at the oil control ring while reducing the ring width causes a decrease in the

film thickness.[23] Harigaya et al.[24] found from his experimental investigation that increasing the engine speed and the oil viscosity, or decreasing temperature can achieve a thicker oil film.

Abu-Nada et al.[25] approximated the shape of the oil film thickness with the minimum oil film thickness values occurring at BDC and TDC, while higher values occurred in mid-stroke, with film thickness ranging from 2.5 to 8 μm in the power stroke at idle speed with SAE 10W50 oil and at an engine speed of 1600 r/min. The friction performance and wear behavior during breaking-in are affected by adsorption and surface reactions of lubricating oil components.[26] The highest friction value occurs during the firing stroke and increases with engine load. Moreover, the piston skirt friction force reduced significantly with reducing skirt surface roughness.[27] The friction can significantly alter the shape and decrease the size of the plastically deformed region in the asperity in the case of fully plastic contact.[28] In boundary and mixed lubrication the surface texture plays a greater role.[29] The fresh lubricants lead to a lower amount of running-in wear and a higher steady-state wear rate, whereas the amount of running-in wear is higher for all altered oils, but the steady-state wear rates are much lower than for the fresh oils.[30]

Baker et al.[31] presented the solutions for equations of motion in both the tangential and radial directions to study the effect of in-plane dynamics of thin compression rings on friction in engines. The study then revealed that the rings sealing effect at vicinity of TDC and BDC tended to decrease with an increase of the clearance between the rings and liner, whilst the blow-by gasses tended to increase due to the poor sealing effect of the rings. Nevertheless, blow-by gasses can cause oil dilution and contamination. The results of this analysis show that enhancement of blow-by was due to internal forces deforming the compression ring. However, the minimum oil film thickness was also reduced, which may increase friction and wear at TDC and BDC locations.

Tian et al.[32] established a ring dynamics and gas flow model, to study the effects of ring dynamics on wear of ring/liner, wear of ring /groove, and oil consumption in a diesel engine. Ring flutter was observed and its effects on oil transport were discussed. The results revealed that the profile of the worn upper wedge of the top ring was critical for oil consumption and its running surface can scrap oil from the liner on the anti-thrust side during the latter part of the compression stroke. Furthermore, during ring flutter, the gas is blown down through the second ring/groove clearance and the second land pressure also dropped. Thus a negative twist on the second ring may be beneficial to oil consumption control. On the other hand, a reverse flutter may occur for top ring with a positive static twist under high engine speed and may induce oil flow into the combustion chamber and cause oil loss. The objective of the presented work was to study the effect of piston ring dynamics on basic tribological parameters. This would help in reducing friction as well as making a contribution towards the improvement of engine performance.

Theory and governing equations

Model description

The piston ring dynamics model was used for the simulation of a four-stroke single cylinder diesel engine operating at full load. To analyze effects of piston ring motion, engine speed and oil viscosity on asperity and hydrodynamic friction forces, frictional power losses, oil film thickness and lube oil consumption.

The piston rings pack consists of three rings (see Figure 2), while Figure 3 shows a cross-section of a piston ring. The diagram in Figure 4 shows the pressure curve in the combustion chamber at all engine speeds.

Program input data

The baseline cases selected engine speed from 800 to 7000 r/min during full load with different engine oils. Engine specifications and the basic engine data are given in Tables 1 and 2, respectively.

Lubricant description

The lubricant used in this simulation model of the piston ring dynamics is the SAE 10W40 and SAE 20W40 lubricating oils. The properties of the lubricating oil are shown in Table 3.

Dynamic viscosity. The temperature variation of viscosity was assumed to be according to that described by Vogel's equation

$$\eta_o = A \exp\left(\frac{\mathrm{B}}{T + C}\right) \tag{1}$$

where η_o is the dynamic viscosity of engine oil, T is the temperature of oil, A, B, and C are constants for a given lubricant (Vogel Parameters) used in the study and have been given in Table 4.

The moments and mechanical forces acting on the piston

The piston ring primary motion is defined by the motion of the piston. First of all, it is the reciprocating motion along the cylinder axis. During the operating cycle of the engine certain moments and lateral forces are generated, which act on the piston as shown in Figure 5. This causes the piston secondary motion due to the presence of small clearance between the piston and cylinder liner. The characterization of the

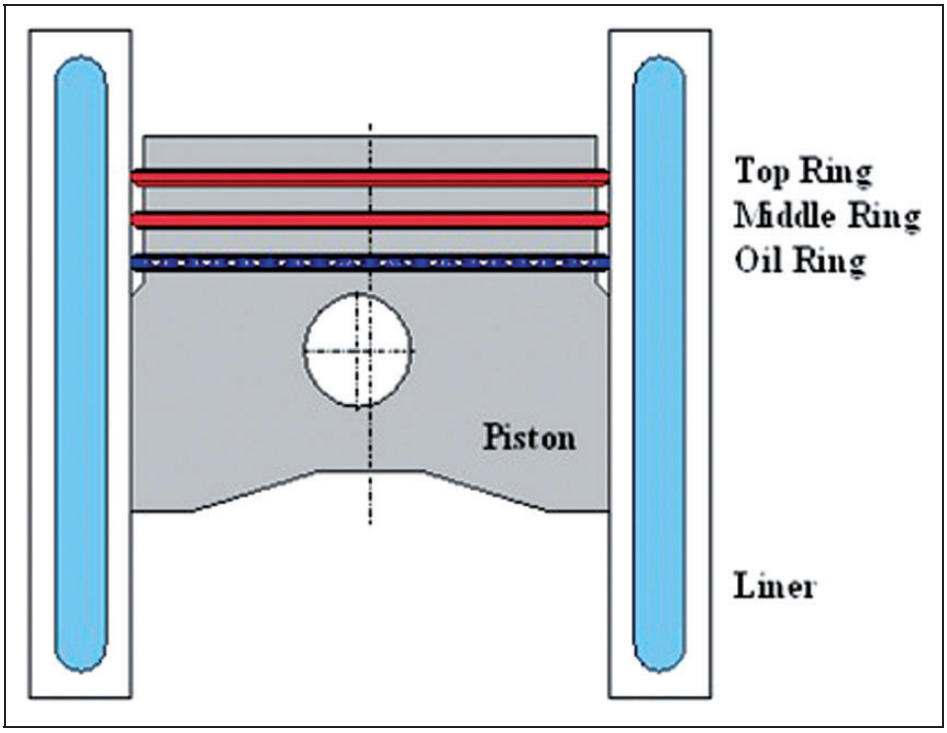

Figure 2. Schematic of the piston rings assembly.

dynamic relationships is based on the equilibrium of moments and mechanical forces in respect of the center of gravity of the piston. According to the equilibrium of dynamic forces acting at the piston, the equations of motion are given by

Forces acting in axial (y) direction

$$\sum F_y = F_{gas} + F_{f\,ring} + F_{f\,skirt} + F_{inertial\ pin\_y} + F_{inertial\ piston\_y} + F_{rod}\cos\theta = 0 \tag{2}$$

Forces acting in radial (x) direction

$$\sum F_x = F_{skirt} + F_{inertial\ pin\_x} + F_{inertial\ piston\_x} - F_{rod}\cos\theta = 0 \tag{3}$$

$$\sum M = M_{skirt} + M_{inertial\ piston} + M_{inertial\ piston\_x}(\alpha - \beta) + F_{inertial\ piston\_y}C_g + F_{gas}C_p + F_{f\,ring}C_p + M_f skirt + M_{f\,pin} = 0 \tag{4}$$

Eliminating F_{rod} from equations (2) and (3) and considering that piston inertial forces are calculated from the following equations

$$F_{inertial\ piston\_y} = -m_{piston} \cdot \ddot{Y} \tag{5}$$

$$F_{inertial\ pin\_y} = -m_{pin} \cdot \ddot{Y} \tag{6}$$

In the radial direction, inertial forces and moment depend on the piston acceleration as reported by Gohar and Rahnejat.[33]

$$F_{inertial\ piston\_x} = m_{piston}\left[\ddot{e}_t + \frac{\beta}{L}(\ddot{e}_t \ \ \ddot{e}_b)\right] \tag{7}$$

$$F_{inertial\ pin\_x} = m_{pin}\left[\ddot{e}_t + \frac{\alpha}{L}(\ddot{e}_b - \ddot{e}_t)\right] \tag{8}$$

$$M_{inertial\ piston} = I_{piston}(\ddot{e}_t - \ddot{e}_b)\ /L \tag{9}$$

The main characteristics of the piston ring dynamics model

1. Each ring is modelled as a single mass. Twisting, (including pre-twist angle) is considered.
2. The total friction between rings and liner comprises viscous friction due to shear in the lubricant described by Reynolds equation and asperity friction at contact locations described by the Greenwood–Tripp rough surface asperity contact.
3. The modeling of piston ring friction by the solution of the equations of motion by considering equilibrium conditions of moments and forces for each ring. The solution leading to the dynamic components of motion of the rings is carried out by means of explicit integration methods in the time domain. In order to determine the hydrodynamic pressure distribution between the ring running surface and liner, Reynolds' equation is solved iteratively in each time step.

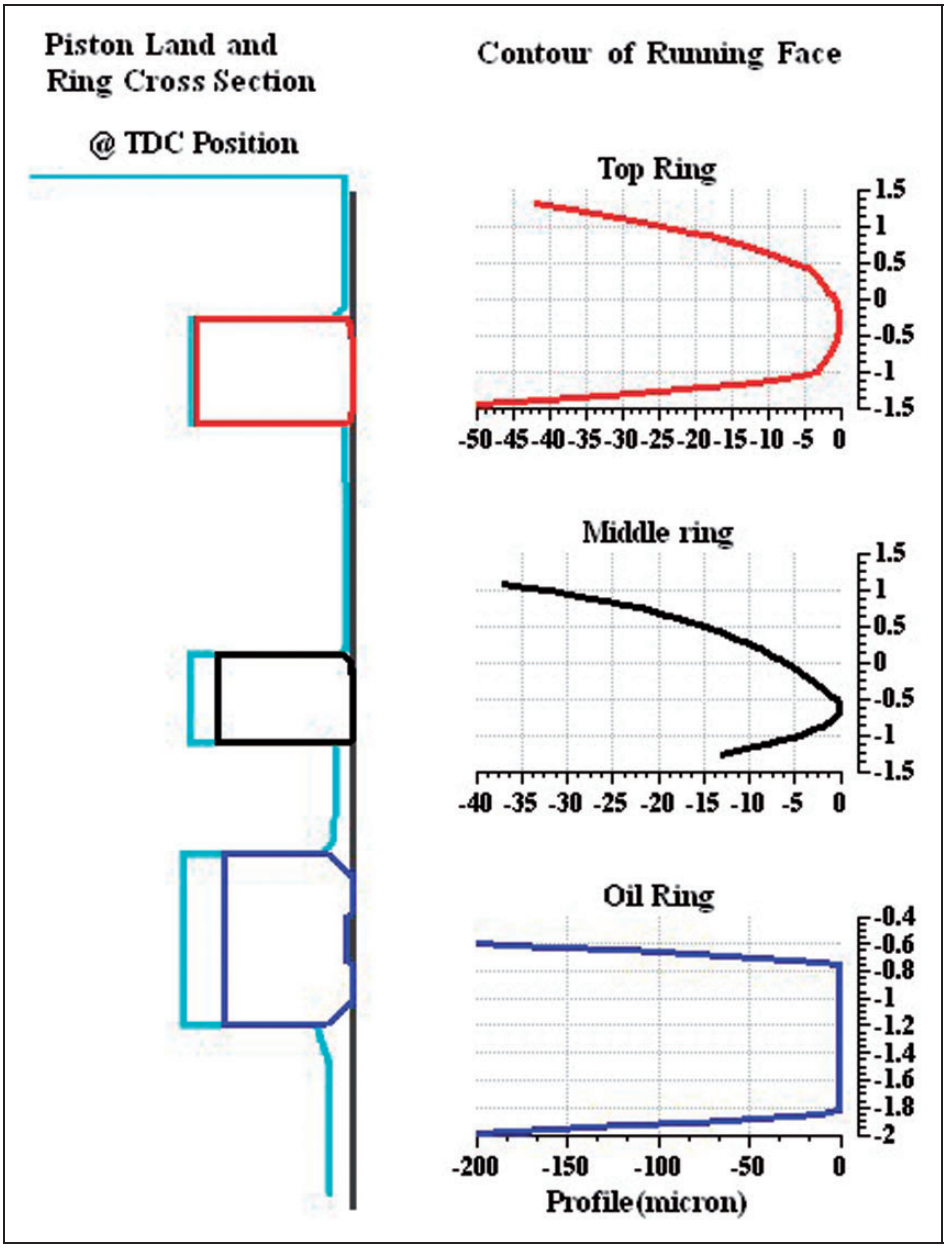

Figure 3. Profile of running face for piston rings.

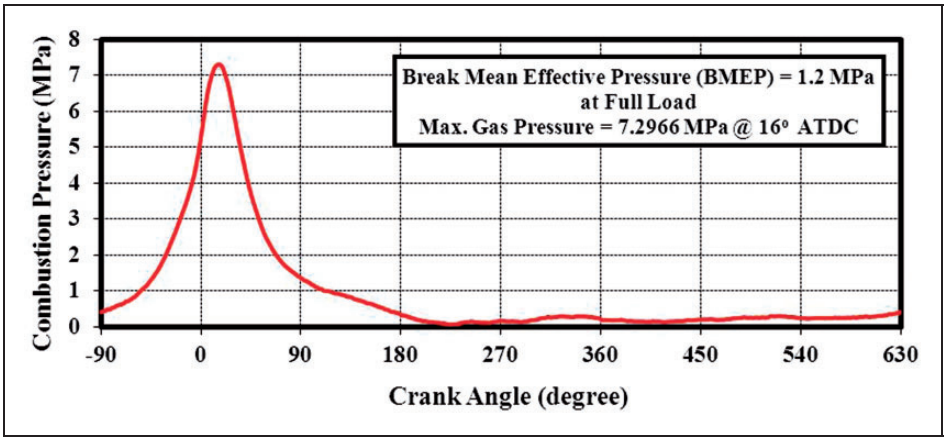

Figure 4. Combustion gas pressure versus crank angle.

4. For the calculation of the gas flow through the rings inter-ring areas are considered as volumes, which are given by the piston and ring geometry and the actual clearances between piston and liner. The volumes are connected due to the actual clearances of ring end gaps and actual position of the rings in the grooves. The possible gas flow behind the rings and between ring and groove flanks is considered.
5. The oil film between the ring running surface and liner is taken into account by calculating the pressure distribution in the clearance according to the liner and ring contours.

Table 1. Engine specifications.

Engine type	Diesel engine
Operating mode	Running
Operating principle	Four-stroke
No. of cylinders	1
Bore (mm)	95
Stroke (mm)	117
Operating speed (r/min)	800–7000

Table 2. Basic dimensions and mass properties.

Parameter	Value
Liner height (mm)	188
Liner thickness (mm)	8
Young's modulus of liner (N/m^2)	9E + 010
Poisson's ratio of liner	0.3
Radial clearance (m)	5E-006
Radial stiffness of liner (N/mm^2)	10,000
Torsional stiffness of liner (Nm/mrad)	10,000,000
Mass of top ring (g)	30.6
Mass of middle ring (g)	22
Mass of oil ring (g)	34
Young's modules (N/mm^2)	90,000
Hardness of piston rings (MPa)	1200
Average temperature of top ring (°C)	200
Average temperature of middle ring (°C)	150
Average temperature of oil ring (°C)	120
Expansion coefficient (1/k)	1.15E-005
Asperity parameter for ring/liner contact: R.M.S surface roughness (micron)	0.2

Assumptions of simulation model

For the simulation of the piston ring dynamics, the following assumptions are made:

1. Radial inertial forces of the rings are neglected because of minor changes caused by oil film thickness and negligible residual radial forces due to good ring-bore conformance.
2. The equation of motion in the radial direction is not solved explicitly; there will only be a calculation as to whether the ring is lifted from the liner wall or not.
3. The radial friction force between piston ring flanks and piston ring groove is calculated by means of the friction function according to Stribeck.
4. The axial damping force is calculated by solving the Reynolds equation taking into consideration rough surface contact.
5. The calculations of the gas flow and pressures are quasi stationary computed by a system of chambers and throttling points. Flow processes are considered as being isothermal. The maximum velocity of flow is limited to the sound velocity at the throttling points.
6. There is no pressure drop in the piston top land, the combustion pressure acting above the top ring.

Table 4. Vogel parameters for different SAE specifications of lube oils.

SAE Specification	A (Ns/m^2)	B (°C)	C (°C)
SAE 10W40	0.132 E-03	737.810	77.700
SAE 20W40	0.093 E-03	1146.250	124.700

Table 3. Characteristics of lubricant oil.

	Atmospheric pressure				200 MPa @ 160°C and 106 s^{-1}	
	@ 40°C		@ 100°C			
Characteristics	SAE10W40	SAE20W40	SAE10W40	SAE20W40	SAE10W40	SAE20W40
Dynamic viscosity (MPa.s)	70.435	97.951	12.286	15.273	4.520	5.212
Density (kg/m^3)	864	864	864	864	864	846
Specific heat capacity (J/kgk)	2083	2083	2083	2083	2083	2083
Thermal conductivity (W/mk)	0.14	0.14	0.14	0.14	0.14	0.14

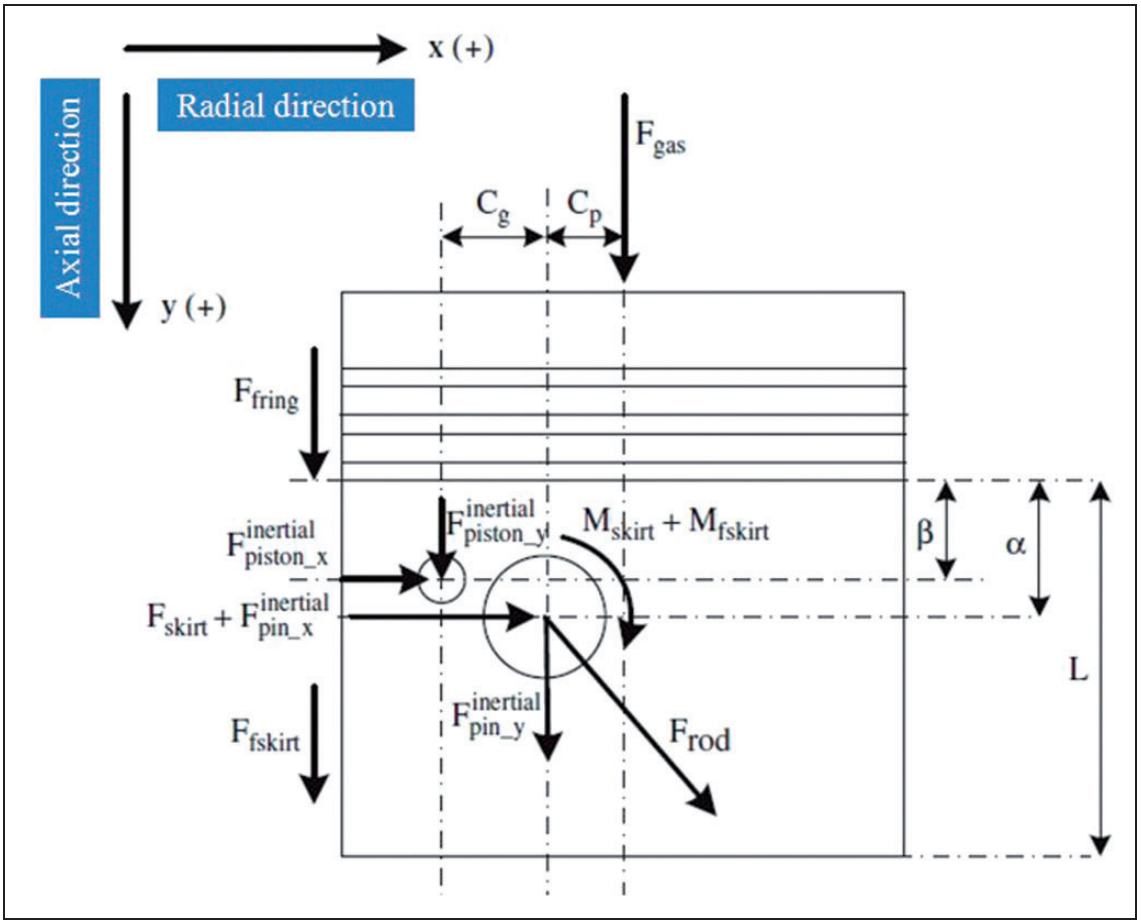

Figure 5. Free body diagram of forces and moments acting on piston.

Below and behind the oil ring, the crankcase pressure is active.

7. The gas pressure distribution in the flank clearance between ring and groove is calculated by assuming the pressure gradient as being inversely proportional to the current clearance.

Governing equations of piston ring dynamics

Figure 6 indicates the forces and moments acting on the piston ring due to gas pressure, inertial effects, and interaction between the piston groove and cylinder liner, as the oil film depends on the contact regime. The model of piston ring dynamics considers forces and moments due to inertia, friction and the flow of the gas from the combustion chamber through the inter-ring volumes into the sump. Piston ring dynamics are influenced by both the twist and tilting motions. The rings are subject to higher variable loading and thus, complex phenomenon fairly in motions.

Axial motion of the piston ring. Axial motion of piston rings in piston grooves appears to be due to the resultant of five acting forces including gas force ($F_{gas,\ ax}$) which is due to the difference in the gas pressure above and below the ring; the inertia force, including gravity and piston tilting motion is due to the change of piston velocity; the friction force ($F_{fric,\ ax}$) due to the friction between the cylinder wall and ring running surface; the bending force (F_{bend}) caused by the interaction between thrust and anti-thrust sides. Damping force ($F_{hydr,\ ax}$) caused by the oil filling of the groove.

In order to judge whether the ring is in contact with the groove flank, contact force between the ring and groove is calculated as

$$F_{contact,\ ax} = F_{inertia,\ ax} + F_{fric,\ ax} + F_{gas,\ ax} + F_{bending} \tag{10}$$

If $F_{contact,\ ax} > 0 \Rightarrow$ ring is moved with the piston
The axial motion is given by: $Y_{ring} = Y_{piston}$
If $F_{contact,\ ax} \leqslant 0 \Rightarrow$ lifting of the ring from groove flank

According to the equilibrium of dynamic forces acting upon the ring, the equation of motion in axial direction is given by

$$m_{ring}\ \ddot{Y}_{ring} = F_{gas,\ ax} + F_{fric,\ ax} + F_{hydr,\ ax} + F_{bending} \tag{11}$$

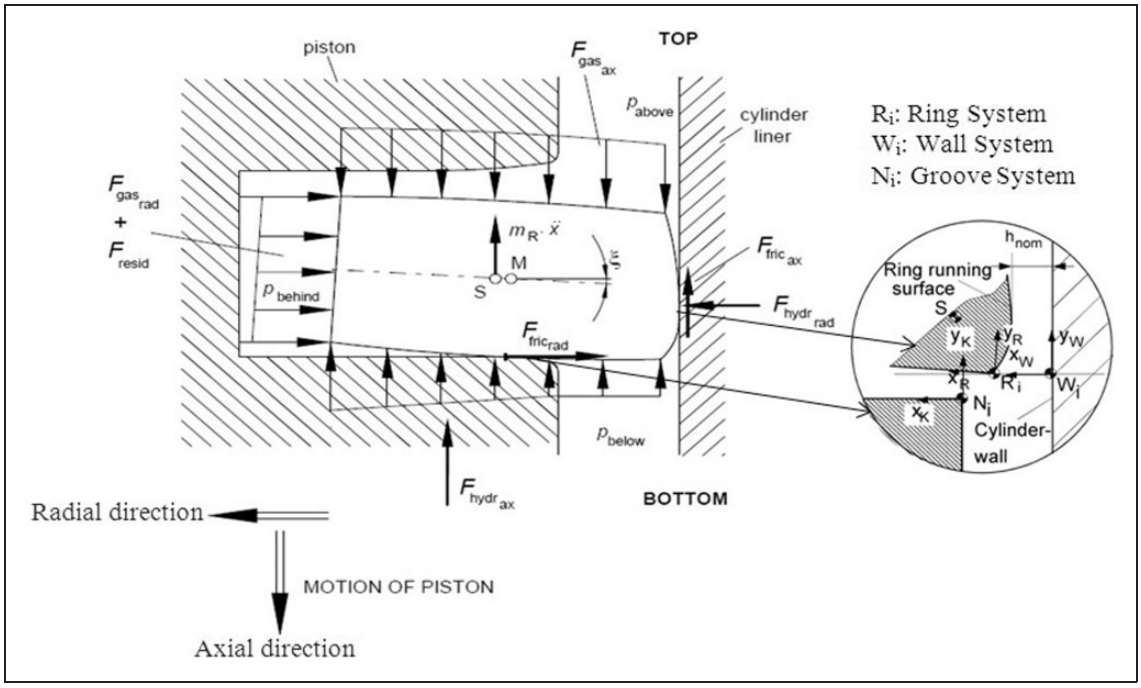

Figure 6. Coordinate systems and forces within the ring system.

Radial motion of the piston ring. The contact forces between the cylinder liner and piston ring running surface is calculated as

$$F_{contact,\,rad} = F_{gas,\,rad} + F_{tension} + F_{fric,rad} + F_{hydr,\,rad} \tag{12}$$

If $F_{contact,\ rad} \leqslant 0 \Rightarrow$ lifting of the ring from liner.

As mentioned earlier, the equation of motion in radial direction is not solved explicitly because of residual radial force negligible due to good ring-bore conformance. However, the equations of motion in both the tangential and radial directions could be solved in accordance with equations (13) and (14) as reported by Baker et al.[31]

$$\frac{\partial^6 v}{\partial\varphi^6} + 2\frac{\partial^4 v}{\partial\varphi^4} + \frac{\partial^2 v}{\partial\varphi^2} + \frac{1}{p\omega_o^2}\frac{\partial^4 v}{\partial\varphi^2\,\partial t^2} - \frac{1}{p\omega_o^2}\frac{\partial^2 v}{\partial t^2} = \frac{a^3}{EI}\left\{\frac{\partial^2}{\partial\varphi^2}\left[F_R(\varphi,t)\right] - \left[F_T(\varphi,t)\right]\right\} \tag{13}$$

$$\frac{\partial^6 w}{\partial\varphi^6} + 2\frac{\partial^4 w}{\partial\varphi^4} + \frac{\partial^2 w}{\partial\varphi^2} + \frac{1}{p\omega_o^2}\frac{\partial^4 w}{\partial\varphi^2\,\partial t^2} - \frac{1}{p\omega_o^2}\frac{\partial^2 w}{\partial t^2} = \frac{a^3}{EI}\left\{\frac{\partial^2}{\partial\varphi^2}\left[F_R(\varphi,t)\right] - \frac{\partial}{\partial\varphi}\left[F_T(\varphi,t)\right]\right\} \tag{14}$$

More recently, the homogeneous parts of equations (13) and (14) have been solved by Baker et al.[31]

Twisting of the piston ring. For moment equilibrium about the center of the cross-section (Point M in Figure 6)

$$\Sigma M = \Sigma(F_{inertia}h_i) + M_{pre-twist} = M_{elastic}\xi \tag{15}$$

where h_i is the moment arm for each force component and ξ is the twist angle.

Hydrodynamic and asperity contact model. The hydrodynamic (viscous friction) in lubricant film and shearing of asperities creates the friction force in the mixed lubrication regime. Total friction force between the piston ring and the cylinder liner is calculated as follows

$$F_{friction} = F_{Asperity} + F_{Hydrodynamic} \tag{16}$$

For the hydrodynamic lubrication model the Reynolds equation is used. It is the relationship between the pressure and the film shape as a function of sliding velocity of the piston ring and oil viscosity. Since the oil thickness between the piston ring and the cylinder wall is much smaller than the piston ring radius, the simplified modification of Reynolds equation can be used

$$\frac{\partial}{\partial x}\left(\Phi_x h^3\,\frac{\partial p}{\partial x}\right) = 6\eta_o U\frac{\partial h_t}{\partial x} + 6\eta_o U\sigma\frac{\partial\Phi_s}{\partial x} + 12\eta_o\frac{\partial h_t}{\partial x} \tag{17}$$

where h is the nominal film thickness, h_t is the local film thickness, P is the hydrodynamic pressure, η_o is the oil viscosity, σ is the ring–liner composite surface roughness, Φ_x is the pressure flow factor, Φ_s is the shear flow factor, and U is the sliding velocity of the piston ring.

Ring–liner composite surface roughness(σ) is defined as

$$\sigma = \sqrt{\sigma_{liner}^2 + \sigma_{ring}^2} \tag{18}$$

where σ_{liner} and σ_{ring} are the r.m.s surface roughness of the ring and liner, respectively.

For solving Reynolds equation, the solution technique used maintains the boundary conditions according to Reynolds equation and enforces a gradual transition of the pressure into the cavitation zone of the divergent gap area.

The hydrodynamic friction force is given by the integration of the oil film pressure over the ring face oil film pressure distribution

$$F_{Hydrodynamic} = \int \left[\Phi_{fp} \frac{h}{2} \frac{\mathrm{d}p}{\mathrm{d}x} - \left(\frac{h}{h_t} + \Phi_{fs} \right) \frac{\eta_o U}{h} \right] \mathrm{d}A \tag{19}$$

where A is the section area of element, Φ_{fp} is the shear stress factor due to mean pressure, and Φ_{fs} is the shear stress factor due to local roughness.

The Reynolds equation assumes that surfaces are perfectly smooth. The actual ring and liner surfaces consist of a varying degree of asperities and this causes a variation in the calculations of the fluid pressures. However, measurement of these fluid pressures is not practical; hence a method of flow factors developed by Patir and Cheng[34] is used. The factors Φ_x and Φ_s corrects the shear stress formation in the film, and are dependent on the roughness of the surface and the film thickness. This formulates a simple way for solving many different kind of surfaces. Details of flow factors are attached in Appendix 2.

The asperity contact between piston rings and cylinder liner is solved using the Greenwood and Tripp models.[35] Due to the nature of the inputs for the Greenwood–Tripp model, which are impossible to measure, the final equations of the model, which present the asperity contact pressure and the equivalent asperity contact force is given as

$$P_a = \frac{16\sqrt{2}\,\pi}{15} (\sigma\, \beta_s\, \rho_s)^2\, E \sqrt{\frac{\sigma}{\beta_s}}\, F_{5/2} \left[\frac{h_t}{\sigma} \right] \tag{20}$$

$$F_{5/2} = \begin{cases} 4.4086^{-5} \left(4 - \frac{h_t}{\sigma}\right)^{6.804}, & \frac{h_t}{\sigma} < 4 \\ 0, & \frac{h_t}{\sigma} \geqslant 0 \end{cases} \tag{21}$$

The elastic behavior of the rough surfaces is given by the composite elastic modulus and can be expressed as follows

$$E = \frac{1}{\left(\frac{1-\nu_1^2}{E_1} + \frac{1-\nu_2^2}{E_2} \right)} \tag{22}$$

where E_1, E_2 are ring and liner Young's modulus, β_s is the composite mean radius of curvature of asperity tops, ρ_s is the composite asperity density, and ν_1, ν_2 are ring and liner Poisson's ratio, respectively.

The asperity friction force is given by

$$F_{Asperity} = \mu_b W_a \text{ and } W_a = P_a A_a \tag{23}$$

$$W_a = \int_{-B/2}^{B/2} P_a \, \mathrm{d}x \tag{24}$$

where W_a is the total asperity contact load, A_a is the apparent contact area, B is the ring axial thickness, and μ_b is the friction coefficient during the boundary lubrication regime.

The coefficient of friction (μ) for this model has been directly determined by the following empirical relationship

$$\mu = a_4 D^4 + a_3 D^3 + a_2 D^2 + a_1 D + a_0 \;\&\; D = \frac{\eta_{o,\,mean.} U}{F_n / L_{RW0}} \tag{25}$$

where D is a nondimensional parameter also known as the duty parameter, $\eta_{o,\,mean.}$ is the mean dynamic viscosity of the lubricant (Pas), U the sliding speed (m/s), F_n the normal load (N), L_{RW} the characteristic length (m), and a_4, a_3, a_2, a_1, a_0 constant friction parameters (see Figure 7).

Lube oil consumption model. The lube oil consumption model considers the following lube oil consumption mechanisms: evaporation at the oil film from the liner surface, oil transport around the first piston ring including oil throw off, oil blow through the gap of the first ring from and into the combustion chamber and oil scraping at the top land's top edge (see Figure 8).

The evaporation of lube oil from the cylinder liner wall is defined by mass transfer over the phase boundary in the medium of combustion gas with certain gas turbulence. Figure 9 shows the oil surface which is exposed to the hot gases. In steady-state convective mass transfer applied to simulate the evaporation rate is given by

$$\dot{m} = \frac{\beta_t}{R_{film} T_{film}} (P_{film} - P_{gas}) = -\frac{S}{R_{film} T_{film}} \frac{\mathrm{d}p}{\mathrm{d}r} \tag{26}$$

where β_t is the mass transfer number, R_{film} the gas constant, T_{film} the oil layer temperature, P_{film} the oil vapor pressure, P_{gas} the combustion pressure, and S is the coefficient of diffusion.

For the simulation of the throw-off quantity of the accumulated oil between the piston top land and the liner wall the model involving the division of the entire film into discrete layers was used. Within these layers a constant acceleration is assumed. Between the layers the shear stress according to Newton is acting. By means of the equilibrium of forces at each layer the velocity distribution at the layers can be determined. The thrown-off oil volume can be estimated by

$$V_{throw-off} = (u_m - u_{st,m}) h_{film} d_{film} \pi \Delta t \tag{27}$$

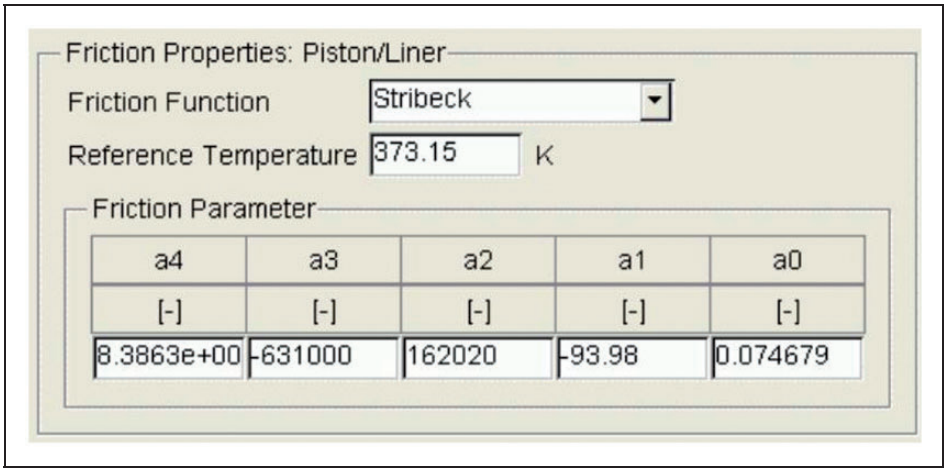

Figure 7. Friction properties piston/liner-Stribeck.

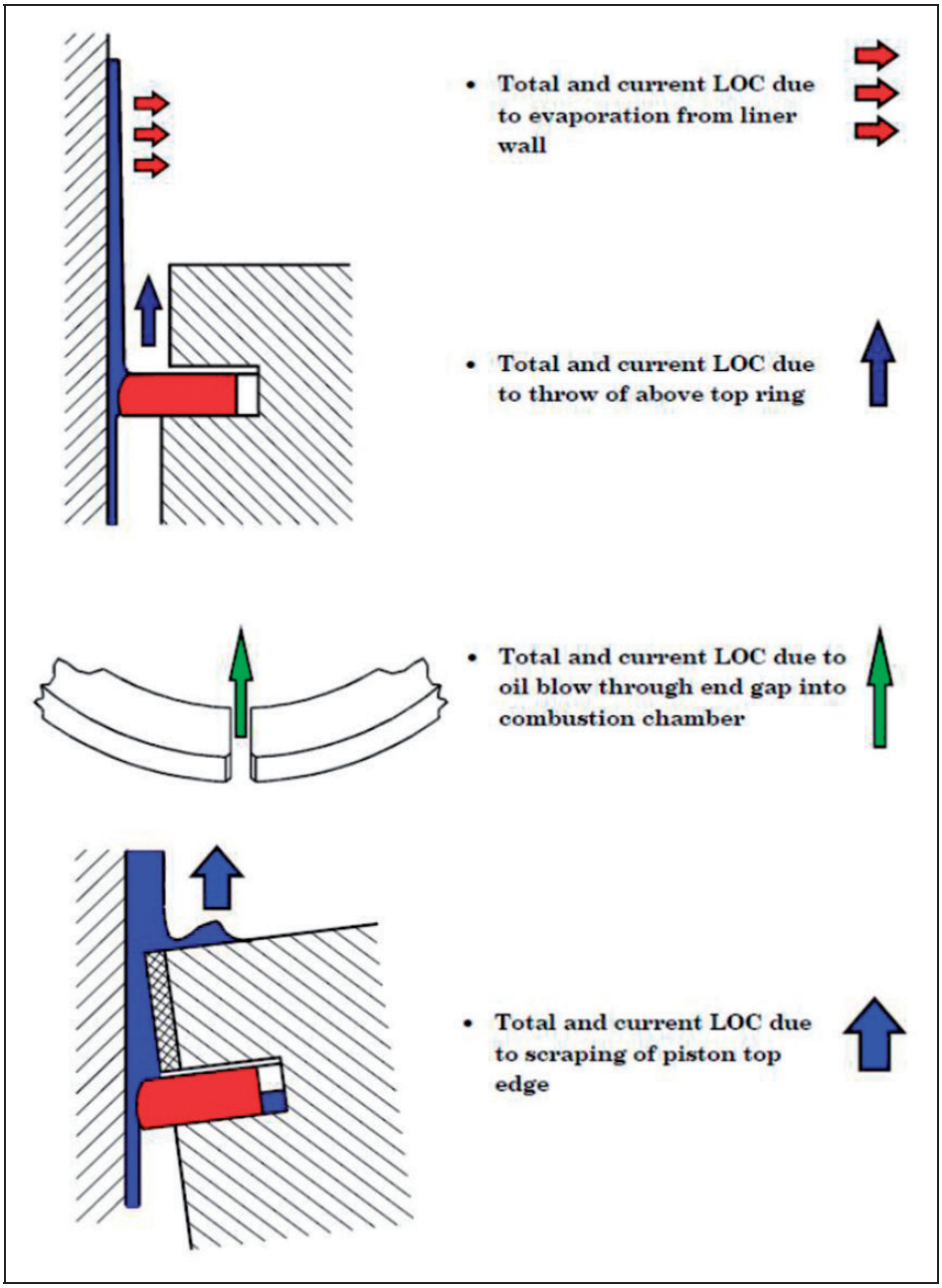

Figure 8. Sources are considered lube oil consumption model.

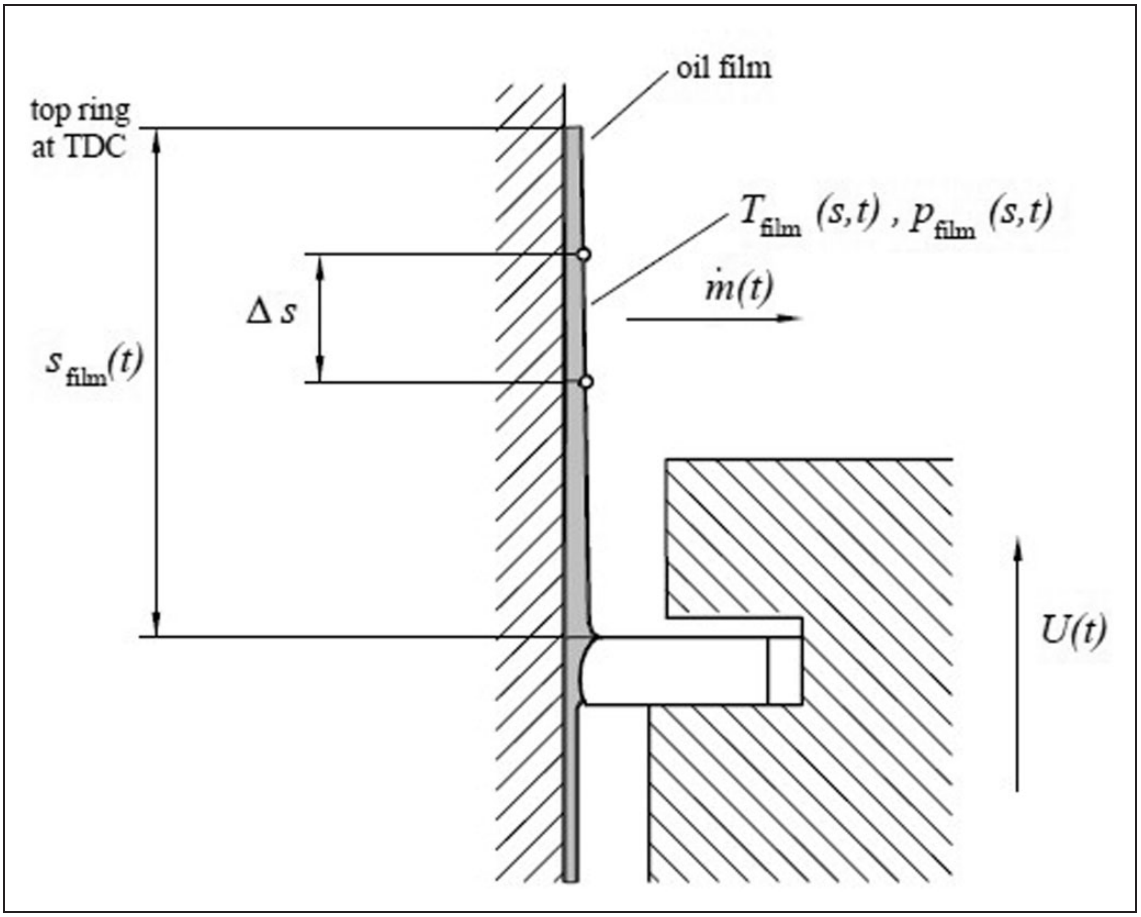

Figure 9. Evaporation model and temperature gradient from liner wall to combustion gas.

where h_{film} is the height of the oil film between top land and liner, d_{film} the diameter at oil film, u_m is the mean instationary velocity, $u_{st,m}$ the mean stationary velocity, and Δt is the time increment.

Results and discussion

Friction force and power losses in an individual piston ring

For the single-cylinder diesel engine, there were four strokes. The crank angle in −90°:0° represents the end of the compression stroke, 0°:180° the expansion stroke, 180°:360° exhaust stroke, 360°:540° intake stroke, and 540°:630° represents the start of the compression stroke.

Figure 10 shows the model results of the friction force values of the individual piston rings against engine crank angle at full load, with a lubricating mineral oil of SAE 20W40 and engine speed of 4000 r/min. The total friction between piston rings and cylinder liner consists of hydrodynamic friction due to lubricant shearing and asperity friction at TDC and BDC. The negative part of the curve is due to the change of piston speed direction through the reciprocating motion. It has been observed that the highest friction force value occurred during the expansion stroke (0°:180°) with a peak of 42 N just after TDC firing. Generally asperity friction force reached its peak at TDC and BDC locations during piston motion, owing to the low critical speed, and hence, the weak access of oil at these locations. However, the hydrodynamic friction increased at mid-stroke. The comparison of the individual piston rings (top ring, middle ring, and oil ring) showed that the top ring had the highest values of friction force at TDC and BDC, while oil ring showed highest values of friction force at mid-stroke due to the enhancement of hydrodynamic friction. Finally, the middle ring showed lowest values of friction force during the four strokes of the operating cycle.

The variation of power losses with crank angle were seen for different piston rings at full load, SAE 20W40 and engine speed of 4000 r/min (see Figure 11). The power losses were observed to reach its peak at mid-stroke location and passes through zero at TDC and BDC, which might be due to the reciprocating speed of the piston reached its maximum value and hence both oil film thickness and hydrodynamic shear increases at mid stroke. The oil control piston rings gave the maximum value of frictional power losses (~0.9 kW) because of the hydrodynamic friction increase, while the middle piston ring showed lower values of power losses which reached

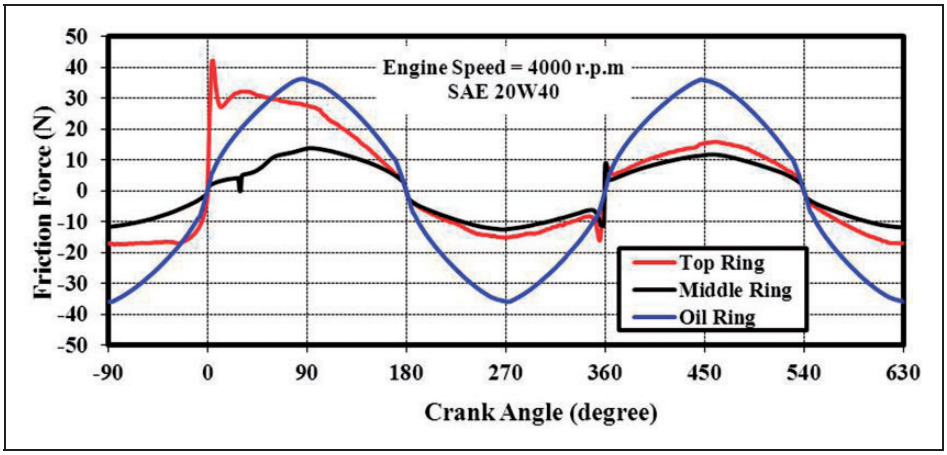

Figure 10. Friction force between piston rings and cylinder liner versus crank angle.

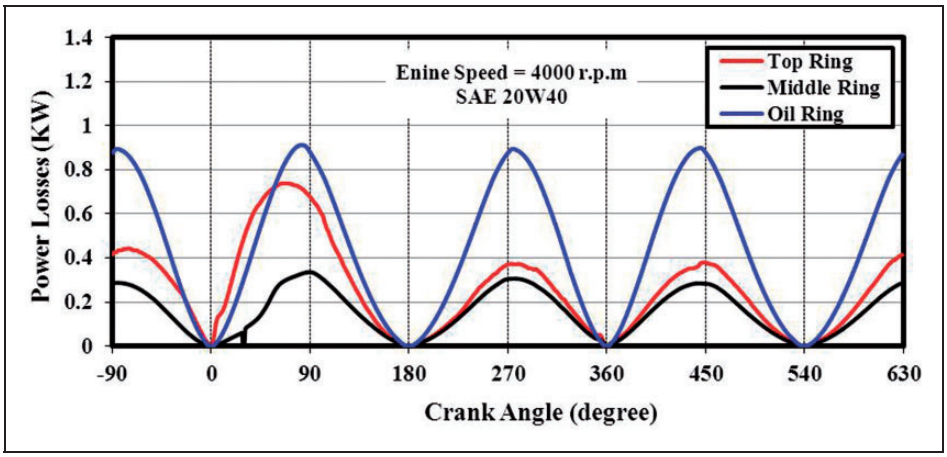

Figure 11. Frictional power losses between piston rings and cylinder liner versus crank angle.

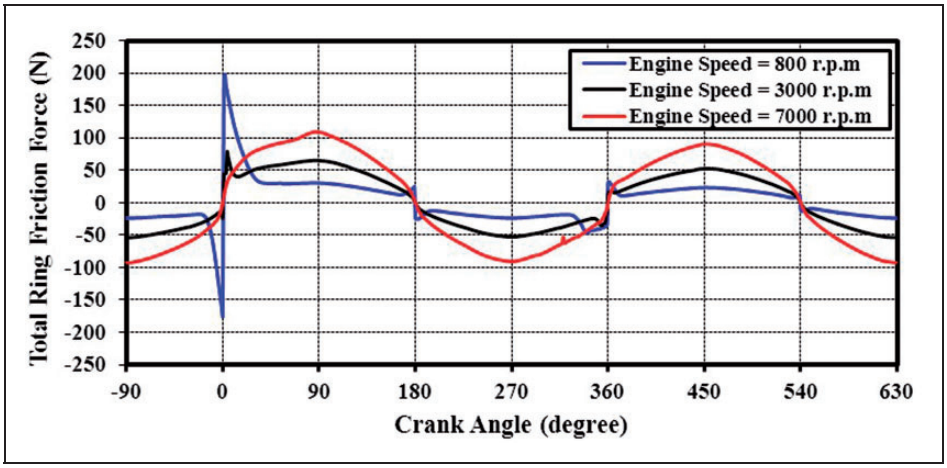

Figure 12. Effect of engine speed on total friction force between piston rings and cylinder liner at SAE 20W40 engine oil.

0.3 kW due to the decrease in hydrodynamic friction and asperity friction. Furthermore, regarding the power losses of the top piston ring, the highest friction force values occurred during the expansion stroke.

Effect of engine speed

Figure 12 demonstrates the impact of engine speed on total friction force between piston rings and cylinder liner with SAE 20W40 engine oil and at full load.

It has been observed that friction force reached its peak (190.5 N) at TDC during the start of the expansion stroke at an engine speed of 800 r/min due to increased asperity (boundary) friction force with a decrease in sliding speed at this location. The results showed that friction force decreased with increasing engine speed at TDC and BDC as a result of increasing oil film thickness between piston rings and cylinder liner. However, a substantial increase of the friction force was recorded at mid-stroke location with increasing engine speed because of the increase in the hydrodynamic friction as a result of the increased shear stress with increasing oil film thickness in mid-stroke. This increase was strongly observed at 7000 r/min.

The variations of frictional power losses with crank angle (see Figure 13) which illustrate the effect of engine speed on frictional power losses. As a general trend, the power losses were observed to reach its peak at mid-stroke where the reciprocating speed reached its maximum and hence the oil film thickness and the hydrodynamic shear being at its minimum at TDC and BDC locations where the speed and oil film thickness are critically low. Moreover, the power losses increase with increasing the sliding speed. This behavior might be attributed to the increase in hydrodynamic shear strength resulting from the increase in the oil film thickness. The maximum frictional power losses during the expansion stroke at mid-stroke for engine speeds of 800, 3000, and 7000 r/min had values of 0.15, 1.23, and 4.8 kW, respectively.

In Figure 14 a comparison of the oil film thickness under varying engine speed from 800 to 7000 r/min against crank angle at full load and with SAE 20W40 engine oil, is illustrated. Generally, the oil film thickness reached its maximum value in the middle of the stroke where there is hydrodynamic lubrication, while the minimum oil film thicknesses tend to be lower at TDC and BDC. These are likely to be the points where the piston ring undergoes metallic contact with the cylinder liner (boundary lubrication). It seems that these effects were more prominent at lower engine speeds than at higher speeds since the combustion gas pressures are relatively high at lower engine

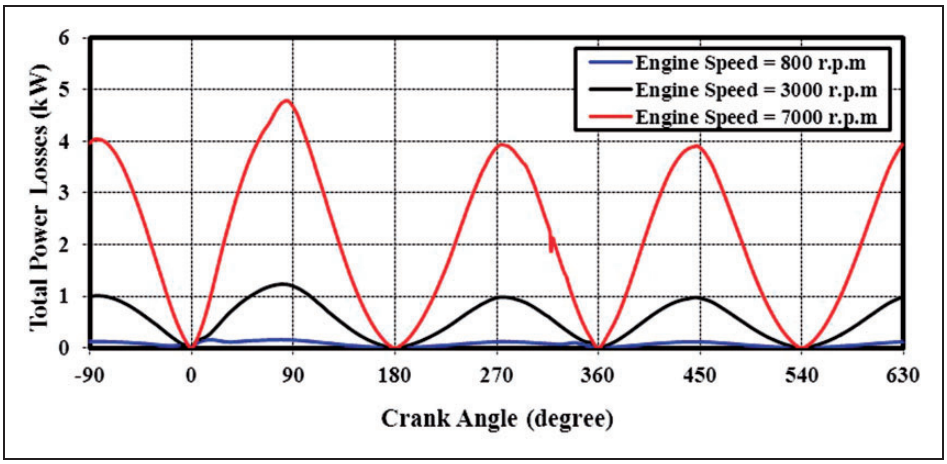

Figure 13. Effect of engine speed on total frictional power losses at SAE 20W40 engine oil.

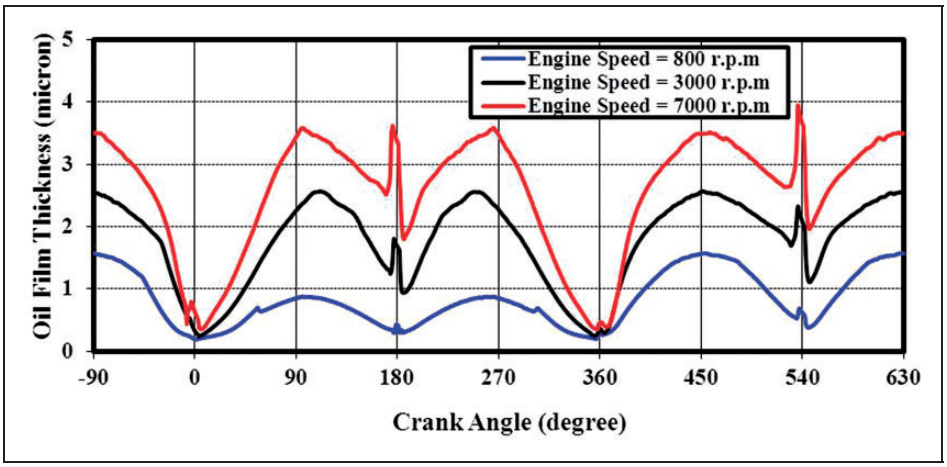

Figure 14. Effect of engine speed on oil film thickness between top ring and cylinder liner at SAE 20W40 engine oil.

speeds. The reason is strongly related to the variation of the reciprocating speed over the whole stroke. In general, the oil film thickness increased with an increase in the engine speed (reciprocating sliding speed). For 800, 3000, and 7000 r/min, the oil film thickness at mid-stroke has been varied from 0.7 to 1.5, 2.4 to 2.6, and 3.4 to 4 μm, respectively.

The effect of engine speed on asperity and hydrodynamic friction forces between the top ring and the cylinder liner was examined with the different engine oils under full load. The asperity friction force showed a considerable decrease in value with increasing engine speed as shown in Figure 15. The reason might be due to the enhancement in oil film thickness which increased the separation between the two rubbing surfaces (ring/liner). Furthermore, asperity friction force decreased with the use of SAE 20W40 engine oil due to the high oil viscosity, but the hydrodynamic friction increased with an increase in engine speed due to the effect of increasing the oil film thickness between the two rubbing surfaces. Hydrodynamic friction force increased with the use of SAE 20W40 engine oil compared with the use of SAE 10W40 engine oil because of an increase in the shear stress.

During engine operation, the piston rings undergo a twisting action due to the interaction with the cylinder liner and this has an influence on the gas pressures. This motion causes a variation in the effective face profile of the ring and a change in the tribological characteristics. The variations of oil ring twist angle against crank angle are presented in Figure 16. The negative direction is due to the upward movement of the piston while the friction force at the oil ring face pushed the oil ring downwards. The results indicated that the twist angle of oil ring was greater than the others near to TDC (0° and 360°) due to high pressure and higher value. Furthermore, fluctuation was also observed because of torsion. Moreover, the increase of the engine speed induced a remarkable increase in twist angle .The twist analysis is very important for the prediction of piston ring dynamics.

Figure 17 shows the axial and radial velocities of the piston ring with crank angle under an engine speed of 4000 r/min. The radial velocity of the piston ring has an important role in the generation of the hydrodynamic force. If the axial velocity of the piston ring is high enough, the majority of the hydrodynamic force is generated by the variable pressure distribution in the ring and piston liner gap. Furthermore, near the piston return points the axial velocity is low and the only hydrodynamic forces are generated by the squeezing effect in which the radial ring velocity plays an important role.

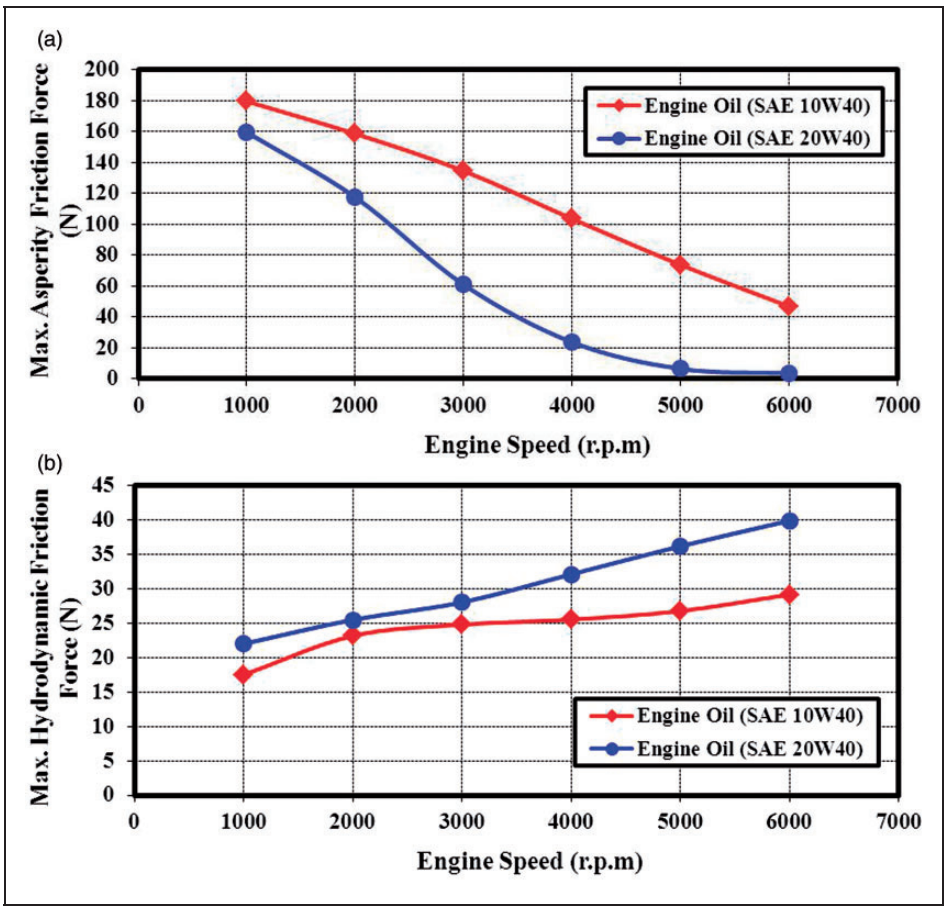

Figure 15. Effect of engine speed on asperity and hydrodynamic friction forces between top ring and cylinder liner at different engine oils.

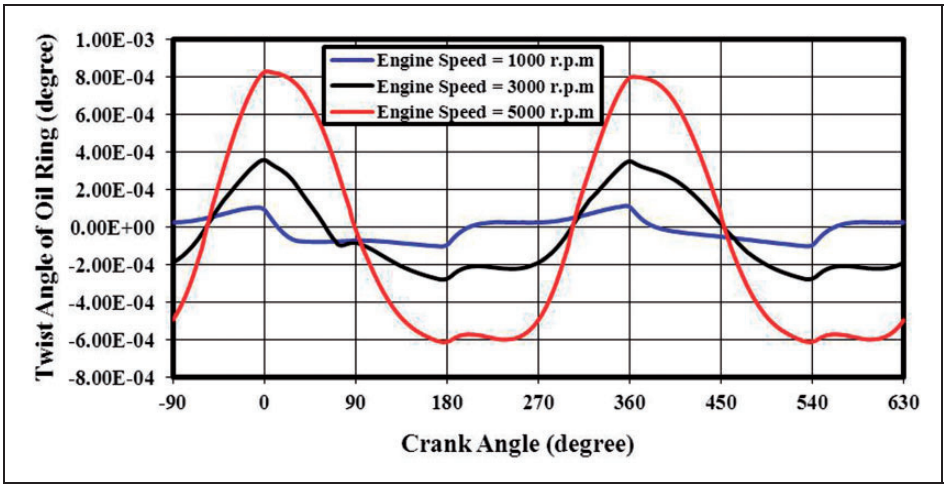

Figure 16. Effect of engine speed on twist angle of oil ring.

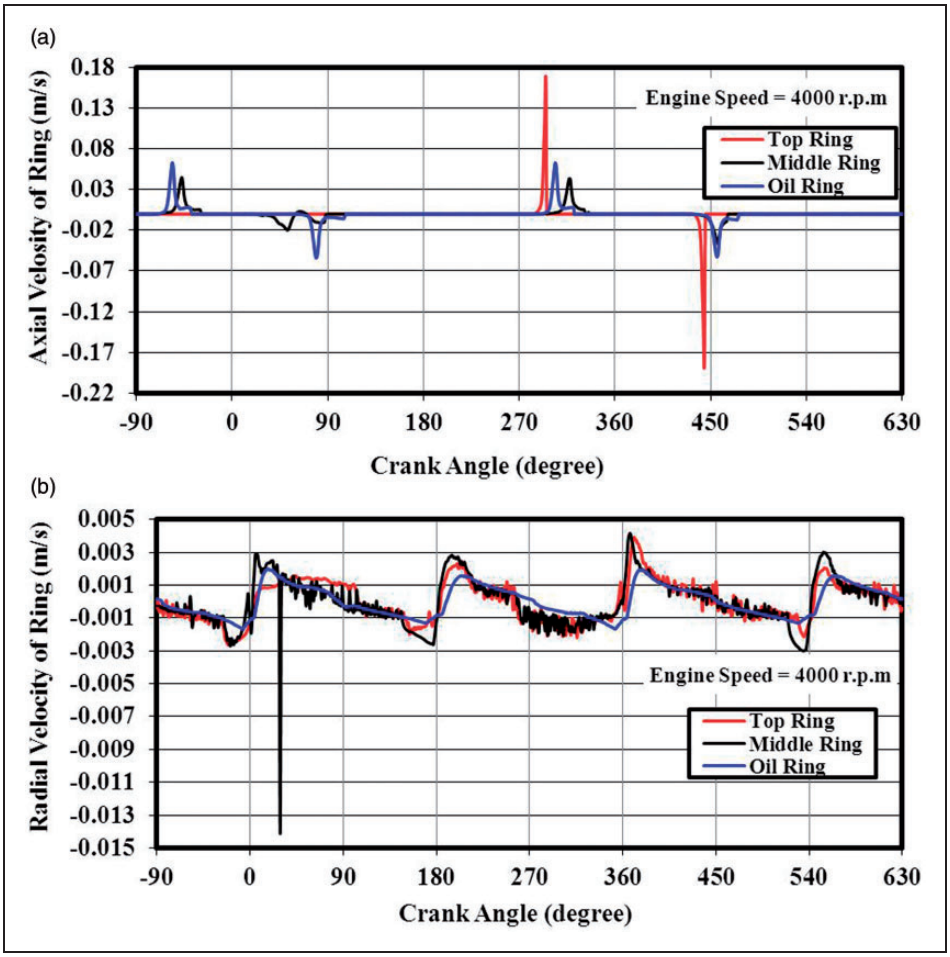

Figure 17. The variation of the axial and radial velocities of the piston ring with crank angle at engine speed of 4000 r/min.

Effect of oil viscosity grades

Asperity and hydrodynamic friction between top ring and cylinder liner against crank angle for an operating engine speed of 5000 r/min and at full load for the different engine oils (SAE 10W40 and SAE 20W40) are presented in Figure 18. It was observed that the peak values of asperity friction force at TDC location (0°:360°) owing to the increase in the metal contact between surfaces (boundary lubrication). However, asperity friction force increased with the use of SAE 10W40 than in the case of SAE 20W40 due to the

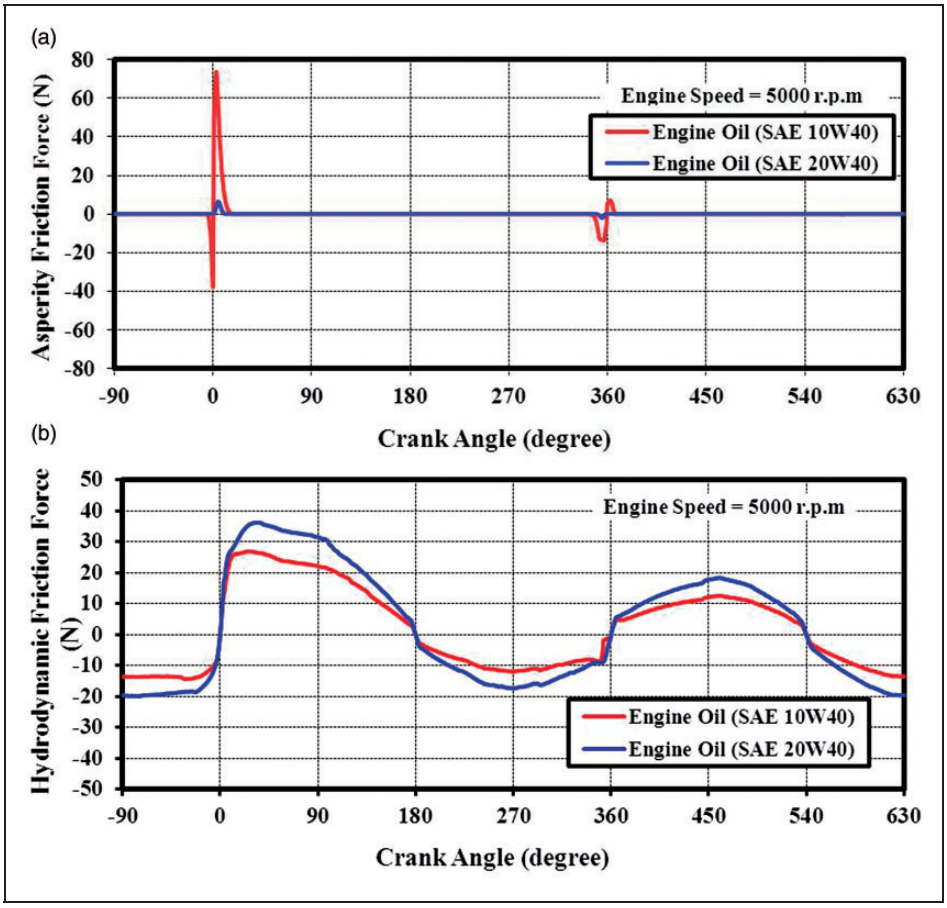

Figure 18. Effect of oil viscosity grade on asperity and hydrodynamic friction forces between top ring and cylinder liner at 5000 r/min.

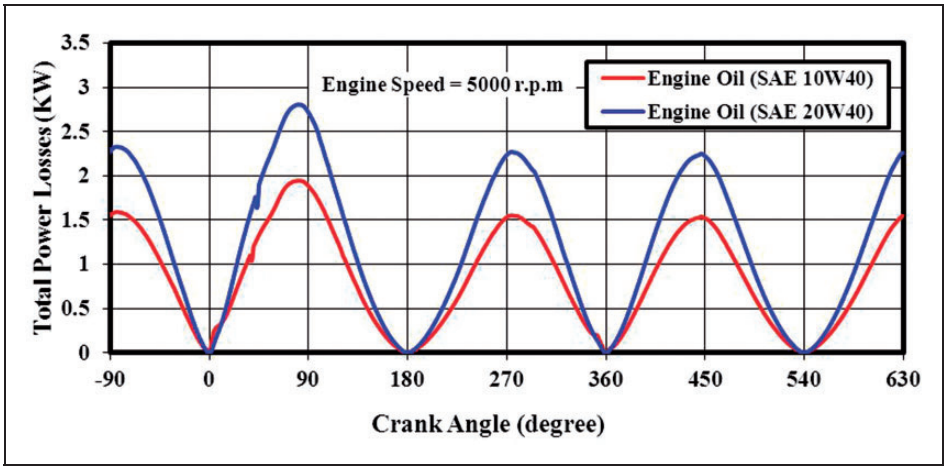

Figure 19. Effect of oil viscosity grade on total frictional power losses at 5000 r/min.

lower oil viscosity. Hydrodynamic friction force also increased with the use of SAE 20W40 than in the case of SAE 10W40. This behavior might be attributed to the increase in shear strength due to the reciprocating speed and oil film increase.

The effect of oil viscosity grade on total frictional power losses and oil film thickness during full load engine at 5000 r/min is shown in Figures 19 and 20, respectively. It was observed that frictional power losses and oil film thickness reached the peak at mid-stroke. The minimum oil film thickness became smaller during the expansion stroke. This phenomenon was more obvious at TDC at the start of the expansion stroke where the oil film thickness reached its minimum. This is mainly a result of the increased cylinder temperature and the high gas pressure at TDC during

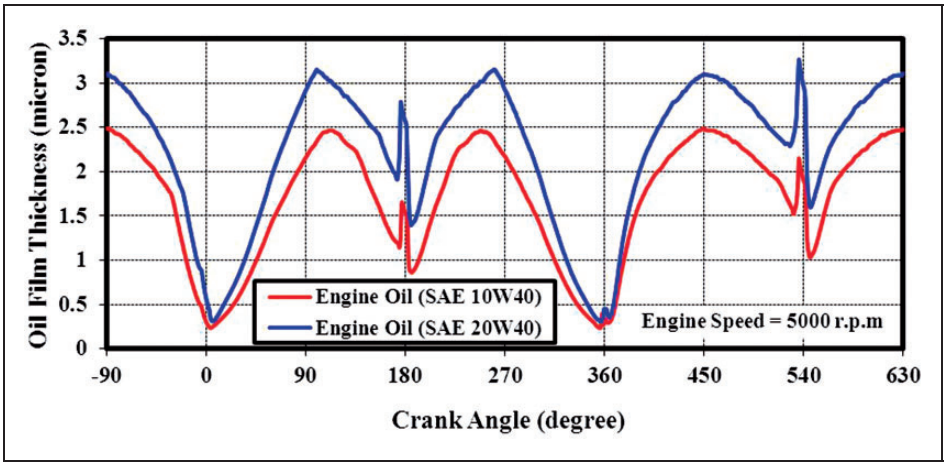

Figure 20. Effect of oil viscosity grade on oil film thickness between top ring and cylinder liner at 5000 r/min.

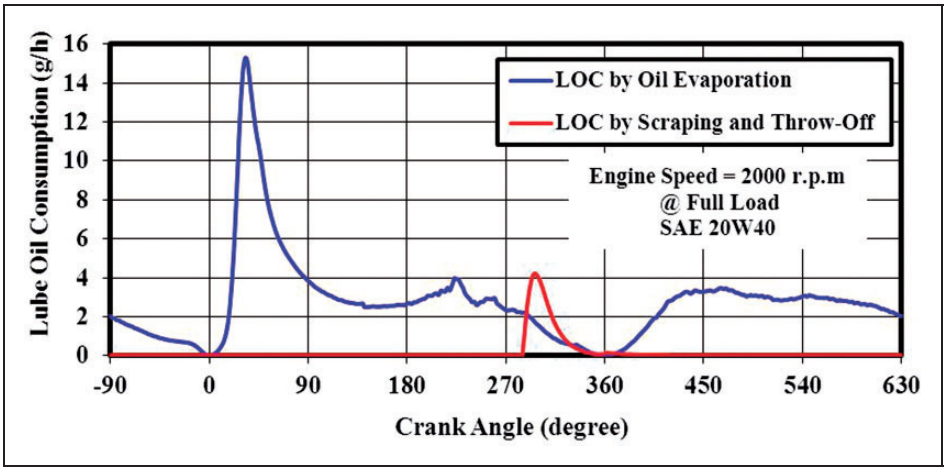

Figure 21. Lube oil consumption by evaporation from liner wall and scraping and throw-off at piston top land versus crank angle.

the expansion stroke which causes a reduction in the oil viscosity. Comparison of the performance of both SAE 10W40 and SAE 20W40, showed that the increase of frictional power losses and oil film thickness in case of SAE 20W40 was strongly related to its high viscosity compared with SAE 10W40. The high viscosity of the SAE 20W40 was substantially responsible for the increase in shear stress in oil film, and could be a strong reason for the increase in hydrodynamic friction with the use of the SAE 20W40 oil.

Lube oil consumption

Figure 21 reveals the relationship between lube oil consumption by evaporation from liner wall, scraping and throw-off at piston top land against crank angle for one cycle of engine operation at 2000 r/min and at full load. The lube oil consumption by evaporation from liner wall was observed to reach its peak at 32° after TDC during expansion stroke. This is attributed to the high-temperature gases and highest thermal loading as it is exposed to the cylinder gases for the longest period during the cycle while lube oil consumption by scraping and throw-off at piston top land might be due to blow-by through top ring end gap. A substantial increase in lube oil consumption by scraping and throw-off was observed with exhaust stroke (180°:360°), with a dominant high values of lube oil consumption being observed at 295° before TDC.

Figure 22 shows the oil consumption rates of each source during one engine cycle along with different engine speeds under SAE 20W40 and at full load. The results showed that increased in lube oil consumption by scraping and throw-off and lube oil consumption by evaporation from liner wall with increasing engine speed was because of reduction in the available time for the gases to flow through the piston-ring pack during one engine cycle. As a result, the increase in the engine thermal loading and increased liner temperatures. The higher values of lube oil consumption by scraping and throw-off after 4000 r/min could be strongly attributed to the increasing engine speed causing higher inertial forces acting on the oil volume that is accumulated on the

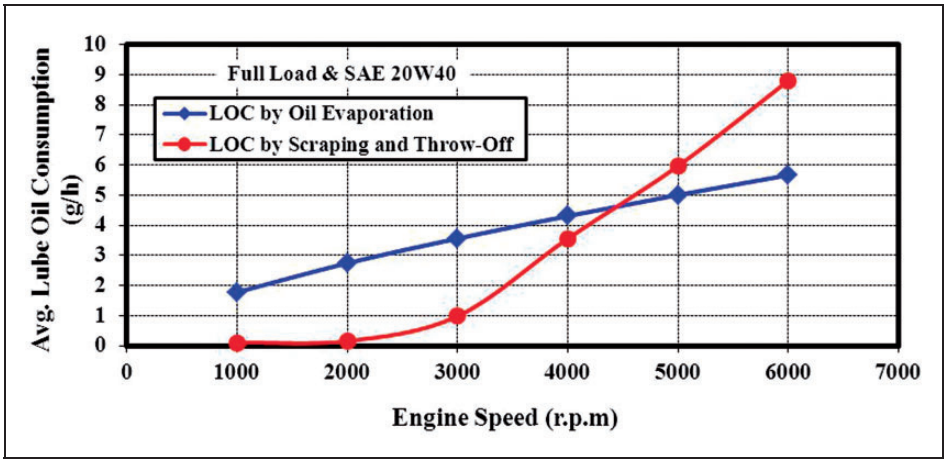

Figure 22. Effect of engine speed on average lube oil consumption during one cycle of engine operation under full load and SAE 20W40.

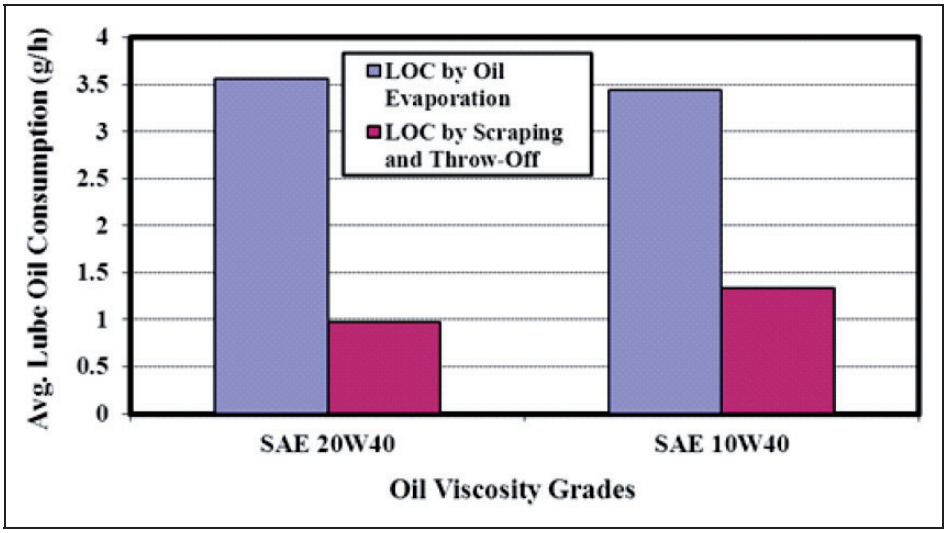

Figure 23. Effect of oil viscosity grades on average lube oil consumption during one cycle of engine operation under full load and 3000 r/min.

piston due to the alternating motion of the piston. The inertia is expected to increase oil flow in the axial direction to the upper piston regions.

In Figure 23 a comparison is made between SAE 10W40 and SAE 20W40 to illustrate the effect of oil viscosity grades on the lube oil consumption by scraping and throw-off at piston top land and the lube oil consumption through evaporation from the liner wall. These results show that the use of the SAE 10W40 oil led to a higher lube oil consumption by scraping and throw-off compared to the SAE 20W40 oil and could be attributed to the low volatility in the SAE 20W40 engine oil.

Conclusions and remarks

The results in current analysis demonstrated that the dynamic behavior of piston rings had a remarkable effect on tribological parameters of the piston ring assembly. The piston ring dynamics change the balance between the asperity (boundary) friction and the hydrodynamic friction contribution to the overall frictional power losses. This is very similar to the Stribeck phenomenon. Hence, an oil viscosity that achieves a balance between the hydrodynamic and boundary lubrication modes is required for minimum friction between rings and liner to help improve the performance of engines. This balance can be achieved using a suitable oil viscosity recommended for the engine. The major remarks that may be drawn from the simulation results are as follows:

1. Asperity friction force (boundary friction) showed high values in vicinity of top and bottom dead centers (TDC and BDC) due to the increase in asperity contact causing thin oil films. However,

at mid-stroke low values were recorded causing thicker oil films, while hydrodynamic friction force dominates in mid-stroke, which can be reduced with a lower oil viscosity.
2. The model predicts the increase in friction power losses, oil film thickness, hydrodynamic friction force, and twist angle of oil ring with an increase in the engine speed whilst the asperity friction force tended to decrease because of the increase in oil film thickness.
3. Oil viscosity directly affects the hydrodynamic friction, with the hydrodynamic friction increasing with oil viscosity. It also influences asperity (boundary) friction indirectly via oil film thickness, but higher oil viscosity causes oil films to be thicker, which reduces the asperity contact.
4. The increase in engine speed (from 1000 to 6000 r/min) at full load (100%) increased the lube oil consumption by scraping and throw-off and lube oil consumption by evaporation from liner wall. Increasing the oil viscosity grade contributes to the reduction of lube oil consumption by scraping and throw-off.

Acknowledgement

The authors appreciate anonymous reviewers for their very helpful comments to improve the manuscript.

Conflict of interest

The authors declared no potential conflicts of interest with respect to the research, authorship, and/or publication of this article.

Funding

The authors would like to express their deep appreciation to the Hubei Key Laboratory of Advanced Technology for Automotive Components (Wuhan University of Technology) for financial support. M. K. A. Ali and R. F. Turkson acknowledge the Chinese Scholarship Council (CSC) for financial support for their PhD studies in the form of CSC grant Numbers 2014GF032 and 2013GXZ993 respectively. M. K. A. Ali also appreciates the financial support from the Egyptian Government.

References

1. Kapsiz M, Durat M and Ficici F. Friction and wear studies between cylinder liner and piston ring pair using Taguchi design method. *Adv Eng Softw* 2011; 42: 595–603.
2. Andersson P, Tamminen J and Sandström CE. Piston ring tribology, A literature survey. VTT Research Notes 2178, 2002.
3. Comfort A. An introduction to heavy-duty diesel engine frictional losses and lubricant properties affecting fuel economy - Part I. SAE Technical Paper 2003-01-3225, 2003. DOI: 10.4271/2003-01-3225.
4. Taylor R. Engine friction: The influence of lubricant rheology. *Proc IMechE, Part J: J Engineering Tribology* 1997; 211: 235–246.
5. Martini A, Zhu D and Wang Q. Friction reduction in mixed lubrication. *Tribol Lett* 2007; 28: 139–147.
6. Ronen A, Etsion I and Kligerman Y. Friction-reducing surface-texturing in reciprocating automotive components. *Tribol Trans* 2001; 44: 359–366.
7. Takiguchi M, Ando H, Takimoto T, et al. Characteristics of friction and lubrication of two-ring piston. *JSAE Rev* 1996; 17: 11–16.
8. Kunkel S, Werner M and Wachtmeister G. Setting up a measuring device to determine the friction of the piston assembly. *SAE Int J Mater Manuf* 2011; 4: 340–351.
9. Wolff A. Simulation based study of the system piston-ring-cylinder of a marine two-stroke engine. *Tribol Trans* 2014; 57: 653–667.
10. Caciu C, Decencière E and Jeulin D. Parametric optimization of periodic textured surfaces for friction reduction in combustion engines. *Tribol Trans* 2008; 51: 533–541.
11. Reipert P and Voigt M. Simulation of the piston / cylinder behavior for diesel engines. SAE Technical Paper 2001-01-0563, 2001.
12. Xu YF, Yu HQ, Wei XY, et al. Friction and wear behaviors of a cylinder liner–piston ring with emulsified bio-oil as fuel. *Tribol Trans* 2013; 56: 359–365.
13. Durga V, Rao N, Boyer B, et al. Influence of surface characteristics and oil viscosity on friction behaviour of rubbing surfaces in reciprocating engines. In: *Proceedings of Fall technical conference ASME-ICE*, vol. 31, New York, 1998, pp.23–35.
14. Priest M and Taylor C. Automobile engine tribology-approaching the surface. *Wear* 2000; 241: 193–203.
15. Douglas R, Steel J and Reuben R. A study of the tribological behaviour of piston ring/cylinder liner interaction in diesel engines using acoustic emission. *Tribol Int* 2006; 39: 1634–1642.
16. Arumugam S and Sriram G. Effect of bio-lubricant and biodiesel-contaminated lubricant on tribological behavior of cylinder liner-piston ring combination. *Tribol Trans* 2012; 55: 438–445.
17. Bolander NW, Steenwyk BD, Kumar A, et al. Film thickness and friction measurement of piston ring cylinder liner contact with corresponding modeling including mixed lubrication. In: *Proceedings of American Society of Mechanical Engineers internal combustion engine division fall technical conference*, 2004, pp.811–821.
18. Saad P, Kamo L, Mekari M, et al. Modeling and measurement of tribological parameters between piston rings and liner in turbocharged diesel engine. SAE Technical Paper 2007-01-1440, 2007.
19. Takata and Rosalind Rosalind Kazuko. *Effects of lubricant viscosity and surface texturing on ring-pack performance in internal combustion engines*. PhD Dissertation, Massachusetts Institute of Technology, USA, 2006.
20. Thring R. Engine friction modeling. SAE Technical Paper 920482, 1992.
21. Richardson DE and Borman GL. Theoretical and experimental investigations of oil films for application to piston ring lubrication. No. 922341. SAE Technical Paper, 1992.
22. Priest M, Dowson D and Taylor C. Predictive wear modelling of lubricated piston rings in a diesel engine. *Wear* 1999; 231: 89–101.
23. Seki T, Nakayama K, Yamada T, et al. A study on variation in oil film thickness of a piston ring package:

Variation of oil film thickness in piston sliding direction. *JSAE Rev* 2000; 21: 315–320.
24. Harigaya Y, Akagi J and Suzuki M. Prediction of temperature, viscosity and thickness in oil film between ring and liner of internal combustion engine. No. 2000-01-1790. SAE Technical Paper, 2000.
25. Abu-Nada E, Al-Hinti I, Al-Sarkhi A, et al. Effect of piston friction on the performance of SI engine: A new thermodynamic approach. *J Eng Gas Turb Power* 2008; 130: 022802.
26. Li S, Zhang R, Jin Y, et al. Competitive surface interactions of critical additives with piston ring/cylinder liner components under lubricated breaking-in conditions. *Tribol Trans* 2003; 46: 200–205.
27. Carden P, Bell D, Priest M, et al. Piston assembly friction losses: comparison of measured and predicted data. No. 2006-01-0426. SAE Technical Paper, 2006.
28. Zhang H, Chang L, Webster M, et al. Effects of friction on the contact and deformation behavior in sliding asperity contacts. *Tribol Trans* 2003; 46: 514–521.
29. Johansson S, Nilsson PH, Ohlsson R, et al. Experimental friction evaluation of cylinder liner/piston ring contact. *Wear* 2011; 271: 625–633.
30. Lenauer C, Tomastik C, Wopelka T, et al. Piston ring wear and cylinder liner tribofilm in tribotests with lubricants artificially altered with ethanol combustion products. *Tribol Int* 2015; 82: 415–422.
31. Baker CE, Theodossiades S, Rahnejat H, et al. Influence of in-plane dynamics of thin compression rings on friction in internal combustion engines. *J Eng Gas Turb Power* 2012; 134: 092801(1)–092801(11).
32. Tian T, Noordzij LB, Wong VW, et al. Modeling piston-ring dynamics, blowby, and ring-twist effects. *J Eng Gas Turb Power* 1998; 120: 843–854.
33. Gohar R and Rahnejat H. *Fundamentals of tribology*. London: Imperial College Press, 2008.
34. Patir N and Cheng HS. An average flow model for determining effects of three-dimensional roughness on partial hydrodynamic lubrication. *ASME J Lubric Technol* 1978; 100: 12–17.
35. Greenwood I and Tripp JH. The contact of nominally flat surfaces. *Proc Instn Mech Engrs* 1971; 185: 625–633.

Appendix I

Notation

a_4, a_3, a_2, a_1, a_0	constant friction parameters
A	section area of element
A_a	asperity contact area
A, B, and C	Vogel parameters of oil
B	ring thickness in axial direction
C_p	distance of the wrist pin from the geometric axis of the piston (wrist pin offset)
C_g	distance of the piston center of mass from the wrist pin axis
d_{film}	diameter at oil film
D	duty parameter
$\ddot{e}_b$	radial acceleration at the bottom of piston skirt
$\ddot{e}_t$	radial acceleration at the top of piston skirt
E	Young's modulus
E_1, E_2	ring and liner Young's modulus
F_{bend}	bending force
$F_{f\ ring}$	friction force of the complete ring pack
$F_{f\ skirt}$	friction force of the piston skirt
F_{gas}	gas force applied on a ring back due to the in-cylinder pressure
$F_{hydr,\ ax}$	damping force caused by the oil filling of the groove
$F_{inertial\ pin\_y}$, $F_{inertial\ pin\_x}$	inertia forces due to wrist pin and connecting rod small end mass
$F_{inertial\ piston\_y}$, $F_{inertial\ piston\_x}$	inertia forces due to piston mass
F_n	normal load
F_R	residual radial force
F_{rod}	force along the connecting rod
F_{skirt}	load capacity of the hydrodynamic fluid film of the piston skirt
F_T	tangential force
h	nominal film thickness
h_{film}	height of the oil film between top land and liner
h_i	moment arm for each force component
h_t	local film thickness
I	second area moment of inertia
I_{piston}	piston rotary inertia about its center of mass
L	piston skirt length
L_{RW}	characteristic length
Lx, Ly	dimensions of unit cell
m_{piston}	mass of piston
m_{ring}	mass of ring
m_{pin}	mass of wrist pin
$\dot{m}$	evaporation rate of lube oil
M_{skirt}	moment about wrist pin due to hydrodynamic forces
$M_{inertial\ piston}$	inertia torque of piston
$M_{f\ pin}$	friction torque of the piston pin
$M_{f\ skirt}$	friction torque of the piston skirt
$M_{elastic}$	elastic moment against ring twisting
$M_{pre\text{-}twist}$	elastic moment due to pre-twist angle
P	hydrodynamic pressure
P_a	asperity contact pressure
P_o	mean hydrodynamic pressure
P_A, P_B	pressure gradient on the boundaries
P_{film}	oil vapor pressure
P_{gas}	combustion pressure
R_{film}	gas constant
S	diffusion coefficient
t	time
T	temperature of oil
T_{film}	oil layer temperature
u_m	mean instationary velocity
$u_{st,m}$	mean stationary velocity
U	sliding speed
v	tangential displacement

$V_{throw\text{-}off}$	thrown-off oil volume
w	radial displacement
W_a	total asperity contact load
X	piston side (secondary) motion
Y	piston translational (primary) motion
α	vertical distance from top of piston skirt to the wrist pin
β	vertical distance from top of piston skirt to the piston center of mass
β_t	mass transfer number
β_s	composite mean radius of curvature of asperity tops
Δt	time increment
η_o	oil viscosity
$\eta_{o,\,mean.}$	mean dynamic viscosity of the lubricant
γ	surface pattern parameter
μ	friction coefficient
$v_1,\ v_2$	ring and liner poisson's ratio
ω	frequency
φ	direction along ring periphery
Φ_{fs}	shear stress factor due to local roughness
Φ_{fp}	shear stress factor due to mean pressure
Φ_s	shear flow factor
Φ_x	pressure flow factor
ρ_s	composite asperity density
σ	ring–liner composite surface roughness
ξ	twist angle
$\emptyset$	connecting rod angle

Appendix 2

Flow factors

Pressure flow factor (Φ_x). The pressure flow factors in the average Reynolds equation can be identified as the correction factors in the pressure flow term to incorporate the effects of surface roughness. The pressure flow factors on a bearing area can be calculated by applying a pressure gradient on the boundaries, solving for the pressure by numerical approach, and then comparing this flow to that of an identical smooth bearing. Hence, considering such bearings of different nominal gaps, the pressure flow factors can be obtained as a function of nominal film thickness. The pressure flow factor Φ_x is then calculated as the ratio of the expected flow in a rough bearing to that in an identical smooth bearing.

$$\Phi_x = \frac{\frac{1}{L_y}\int_0^{L_y} \frac{h_t^3}{12\,\eta_o}\left(\frac{\partial p}{\partial x}\right) \mathrm{d}y}{\frac{h^3}{12\eta_o}\left(\frac{\partial p_0}{\partial x}\right)} \tag{28}$$

where

$$\frac{\partial p_0}{\partial x} = \frac{p_{B-p_A}}{L_x}$$

The pressure flow factors can be presented as a function of the film thickness, roughness ratio, and the surface pattern parameter (γ) of the combined roughness.

$$\Phi_x = \Phi_x\left(\frac{h}{\sigma}\,\gamma\right) \tag{29}$$

Shear flow Factor (Φ_s). Shear flow factor is obtained through numerical simulation. However, no pressure gradient is induced at the boundaries and the rolling velocity is taken as zero. Shear flow factor model is solved for the pure sliding case by Patir and Cheng.

$$\Phi_s = \frac{\frac{2}{L_y L_x}\int_0^{L_y}\int_0^{L_x}\left(-\frac{h_t^3}{12\,\eta_o}\frac{\partial p}{\partial x}\right)\mathrm{d}x\,\mathrm{d}y}{U\,\sigma} \tag{30}$$